JMEPEG (2020) 29:3353–3360
https://doi.org/10.1007/s11665-020-04850-6

©ASM International
1059-9495/$19.00

Micro–Nano Dual-Scale Particle-Reinforced TiB_2/Cu-0.5Cr Composites Prepared by Vacuum Arc Melting

Jiang Feng, Shuhua Liang, Kexing Song, Xiuhua Guo, and Yanjun Zhou

(Submitted December 13, 2019; in revised form April 23, 2020; published online May 22, 2020)

In the present study, a TiB_2 particle-reinforced Cu/Cu-0.5Cr composite was prepared by vacuum arc melting (VAM). The microstructure, mechanical properties and electrical conductivity of the composite after heat treatment were studied. The results show that the micro–nano dual-scale particle-reinforced TiB_2/Cu-0.5Cr (VAM) composite possessed high strength, high hardness and high electrical conductivity. The nano-Cr particles were uniformly dispersed in the copper matrix, and the particle size was below 20 nm. The TiB_2 particles were also uniformly dispersed and had good bonding with the copper matrix. After peak aging at 475 °C for 4 h, the comprehensive properties of the TiB_2/Cu-0.5Cr (VAM) composite were improved. The hardness and electrical conductivity were 99.6 HBW and 82.3% IACS, respectively. The tensile test results show that the tensile strength of the TiB_2/Cu-0.5Cr (VAM) composite was 401 MPa, which is higher than that of the TiB_2/Cu (VAM) composite. The TiB_2/Cu-0.5Cr (VAM) composite had high strength and hardness due to the strengthening of the micro–nano dual-scale particles and the good interface bonding. Based on the tensile fracture morphology of the composite, the failure mechanism of the composite was determined and is discussed.

Keywords copper matrix composite, Cu-Cr, dual-scale, TiB_2, vacuum arc melting

1. Introduction

Copper and copper matrix composites are widely used in many applications that require excellent mechanical properties and electrical conductivity (Ref 1-4). However, the rapid development of transportation, electric power and other industries requires copper matrix composites with improved properties, such as a high softening temperature, high strength, high abrasion resistance and high conductivity. However, obtaining a high electrical conductivity and obtaining high strength in copper materials are contradictory goals. The strengthening approaches for copper materials are based on the introduction of various defects (solute atoms, dislocations, grain boundaries and second phases), and these defects inevitably increase the scattering of conductive electrons, thereby reducing the electrical conductivity (Ref 5, 6). The electronic scattering effect caused by a second phase in a copper matrix is much lower than that caused by a severe lattice distortion caused by solute atoms, and a high strength is obtained while not significantly reducing the electrical conductivity. In addition, compared with solution strengthening and deformation strengthening, second-phase strengthening can significantly improve the softening temperature and wear resistance of the composite. Therefore, among these methods, second-phase strengthening (aging strengthening or dispersion strengthening) is the most effective strengthening approach. The properties of composites depend on the matrix, the reinforcement and the interface bonding between the matrix and reinforcement. In general, pure copper is usually used as the matrix, and the reinforcing phase is a ceramic, such as a carbide, oxide, and boride (Ref 7-11). Although copper matrix composites have suitable properties, especially TiB_2 particle-reinforced copper matrix composites (Ref 12, 13), their strength and hardness still need to be improved. Therefore, alloying elements can be added to pure copper, and the alloy can be used as the matrix for the subsequent composite. This approach can greatly enhance the strength without substantially sacrificing the conductivity. For example, by adding 0.4 $\sim$ 0.6 wt.% Cr into pure copper, the nano-Cr particles can precipitate during the aging treatment, which can greatly increase the strength of the matrix (Ref 14).

The mechanical properties of copper matrix composites are related to the particle size, content and preparation method. Zou et al. (Ref 15) showed that the particle size affects the strength of TiB_2/Cu composites. The smaller the particle size is, the higher the composite strength. You et al. (Ref 16) reported that the tensile deformation and fracture of W/CuCrZr composites were determined by the copper matrix. With the increasing W particle content, the strength is increased, but the elongation is greatly reduced, and the fracture mode changes from ductile fracture to brittle fracture. Bahador et al. (Ref 17) found that the tensile fracture of composites easily occurs where particles are aggregated, and the uniform distribution of particles is the key to preparing a high-strength copper matrix composite. In some of the studies reported in the literature involving dual-scale particle-reinforced Fe-based, Al-based, Mg-based and Ti-based materials, the strength and wear resistance were improved significantly due to synergistic strengthening with different-sized particles (Ref 4, 18-20). Zou et al. (Ref 21) reported that dual-scale particle-reinforced copper matrix composites possessed a higher strength and wear resistance than single-scale

Jiang Feng and **Shuhua Liang**, School of Materials Science and Engineering, Xi'an University of Technology, Xi'an 710048, China; and **Kexing Song, Xiuhua Guo,** and **Yanjun Zhou**, School of Materials Science and Engineering, Henan University of Science and Technology, Luoyang 471003, China. Contact e-mails: fhap256@163.com, liangsh@xaut.edu.cn, kxsong@haust.edu.cn, and guoxiuhua@haust.edu.cn.

particle-reinforced copper matrix composite single-scale composites. Sadoun et al. (Ref 22) observed that Cu-5%ZrO_2/0.5%GNP hybrid nanocomposites can produce a significantly improved hardness and wear rate compared to those of Cu-5%ZrO_2 composites. Therefore, dual-scale processing is an effective way to improve composites properties. However, it is difficult for the traditional preparation approach to obtain the simultaneous presence of dual-scale particles, so it is necessary to develop a new preparation technology. Recently, vacuum arc melting has been used to prepare metal matrix composites (Ref 23-25). Vacuum arc melting can involve rapid melting and rapid solidification in a layer-by-layer manner, which is conducive to obtaining homogeneous and compact composites. Müller (Ref 26) and Li et al. (Ref 27) reported that copper-chromium contact materials were successfully produced using vacuum arc melting technique, the microstructure was homogeneous, and the Cr particles were uniformly distributed. However, no study on dual-scale particle-reinforced copper matrix composites prepared by vacuum arc melting has been reported.

In this paper, TiB_2 particle-reinforced Cu-0.5Cr composites were prepared by vacuum arc melting. The microstructure, hardness, and electrical conductivity of the TiB_2/Cu-0.5Cr (VAM) composite were studied after aging treatment. The strengthening mechanism of the TiB_2 particle-reinforced Cu-0.5Cr composite was determined and is discussed. The fracture mechanism of the composite was analyzed and was combined with an analysis of the tensile fracture morphology.

2. Experimental Procedures

The 5 vol.% TiB_2 particle-reinforced Cu-0.5Cr composites were prepared by VAM. Scanning electron microscopy (SEM) images of commercially available electrolytic copper powder, TiB_2 powder, and chromium powder are shown in Fig. 1(a), (b) and (c). The preparation process is shown in Fig. 1(d) and (e). The fusible electrodes (electrode: Φ70 mm × 700 mm) were sintered at 1020 °C for 3 h in a VQS-5510 vacuum sintering furnace, and the composite (ingot: Φ90 mm × 400 mm) was produced in an L200 arc melting furnace with a voltage of 25 V and a current of 4200 A. For comparison, 5 vol.%-TiB_2/Cu composites were prepared by powder metallurgy (PM) and VAM. The composites were hot extruded into Φ14.5 mm bars at 900 °C. The TiB_2/Cu-0.5Cr (VAM) samples were homogenized and treated for 1 h at 990 °C in a KSSG1200 gas protection tube furnace, followed by quenching in water. Then, the aging temperature was selected as 400-500 °C, and the aging time was 0.5-6 h.

The density of the composites was measured using the Archimedes method, and the relative density (RD) was calculated. The Brinell hardness (BH) of the composites was tested by a 320HBS-3000 Brinell hardness tester (China) with a load of 125 kg and a dwell time of 20 s. The average value of each sample was measured 5 times. The amount of chromium in the composites was measured by a SPECTRO ARCOS ICP spectrometer (Germany). The electrical conductivity of the composites was measured by a Sigma2008B1 eddy current test instrument (China). Tensile tests were performed by a SHIMADZU AG-I250KN precision universal testing machine with a constant strain rate of 2 mm/min. The microstructures and the interface between the particle and copper matrix were observed by a JSM-IT100 SEM (Japan) and a Talos F200X transmission electron microscope (TEM) (America).

3. Results and Discussion

3.1 The Hardness and Electrical Conductivity of the TiB_2/Cu-0.5Cr (VAM) Composite

The variations in the hardness and electrical conductivity of the TiB_2/Cu-0.5Cr (VAM) composites after different aging temperature and aging time treatments are shown in Fig. 2. The results show that the hardness and electrical conductivity of the composite were sensitive to aging temperature. In the early stage of aging, the hardness and electrical conductivity of the composite increased sharply. After increasing the aging time, the hardness reached its peak value and then decreased gently, while the electrical conductivity reached its peak value and then remained basically the same.

The hardness and electrical conductivity of the composite were related to the size, quantity and distribution of the Cr particles. At the early stage of aging, the supersaturation of the alloy is high, the precipitation power and precipitation speed are relatively large (Ref 28, 29); thus, the quantity of Cr particles increases sharply, and the blocking effect on the dislocations is enhanced, resulting in a rapid increase in the hardness. The precipitation of the Cr particles reduced the electron scattering, so electrical conductivity was also improved. At increased aging temperatures or aging times, the Cr precipitates redissolved or coarsened, which decreased the hardness and electrical conductivity of the composites. After peak aging at 475 °C for 4 h, a TiB_2/Cu-0.5Cr (VAM) with improved properties was obtained. The hardness and electrical conductivity were 99.6 HBW and 82.3% International Annealed Copper Standard (IACS), respectively.

The properties of the TiB_2 particle-reinforced copper matrix composite are listed in Table 1. The electrical conductivity of all composites was greater than 82% IACS. The relative density is an important factor that impacts the electrical conductivity and mechanical properties of composites. The electrical conductivity and hardness of the TiB_2/Cu (VAM) composite were higher than those of the TiB_2/Cu (PM) composite because of its higher relative density. The Cr particles dispersed in the copper matrix reduced the mean free path of the electrons and reduced the electrical conductivity of the composite. Therefore, the electrical conductivity of the TiB_2/Cu-0.5Cr (VAM) composite was slightly lower than that of the TiB_2/Cu (PM) composite and the TiB_2/Cu (VAM) composite. However, the hardness of the TiB_2/Cu-0.5Cr (VAM) composite was 81% higher than that of the TiB_2/Cu (VAM) composite due to the strengthening from the aging precipitation.

3.2 Composition Materials and Microstructure

The chromium content in the TiB_2/Cu-0.5Cr (VAM) composite was 0.49 wt.%. The measured chromium content is consistent with the designed theoretical value. The microstructure of the sintered TiB_2/Cu-0.5Cr (VAM) composites is shown in Fig. 1(f). It can be clearly seen from Fig. 1(f) that TiB_2 particles and raw Cr particles were dispersed in the matrix. There was an obvious transition layer between the copper matrix and Cr particles (Fig. 1f), which was due to Cr atoms diffusing into the Cu matrix at the sintering temperature and

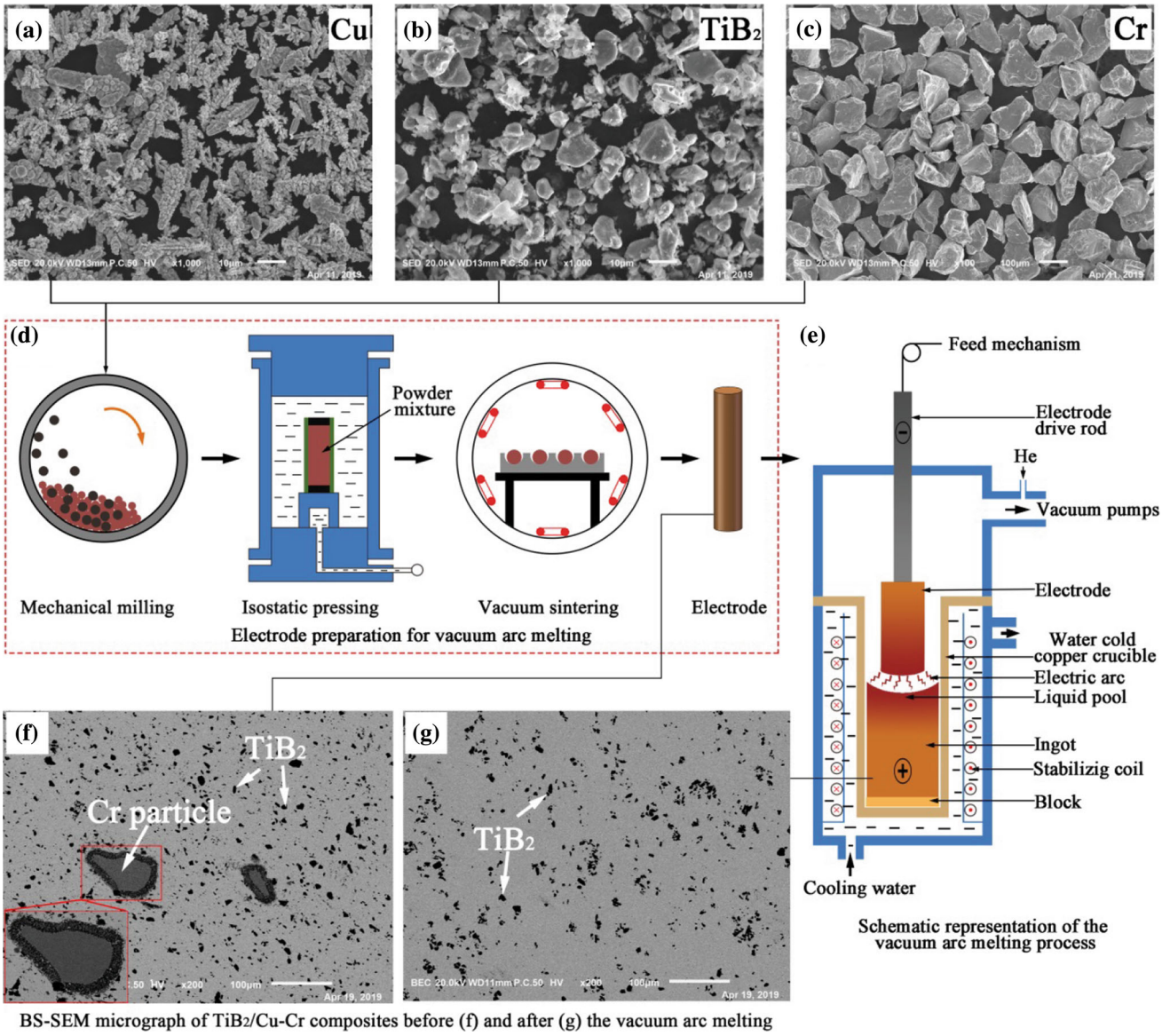

Fig. 1 Schematic representation of the vacuum arc melting process (a) copper powder, (b) TiB_2 powder, (c) Cr powder, (d), (e) electrode preparation and vacuum arc melting process, (f), (g) SEM micrographs of TiB_2/Cu-0.5Cr composite before and after vacuum arc melting

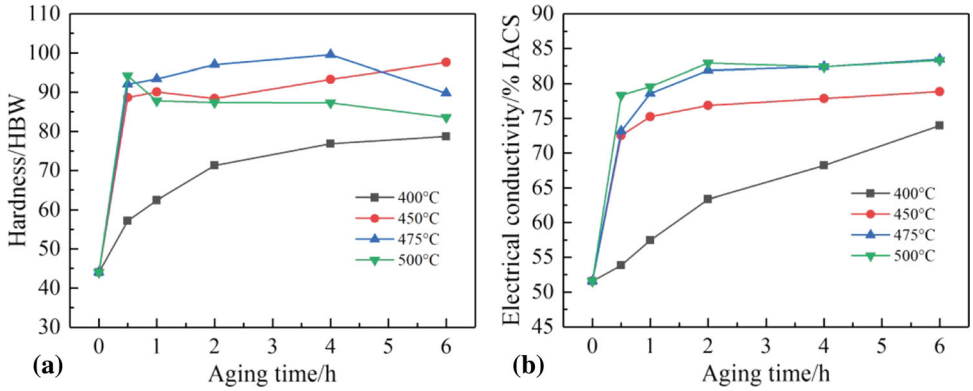

Fig. 2 The hardness and electrical conductivity of the TiB_2/Cu-0.5Cr (VAM) composite aged at different aging temperatures and times

Table 1 Properties of the TiB_2 particles-reinforced Cu and Cu-Cr composites

Composites	RD/%	BH/HBW	YS/MPa	UTS/MPa	El/%	EC/%IACS
TiB_2/Cu (PM)	98.5	50	101	226	24.6	84.6
TiB_2/Cu (VAM)	99.8	55	91	246	38.3	87.0
TiB_2/Cu-0.5Cr (VAM)	99.8	99.6	323	401	23.2	82.3

then precipitating to form Cu-rich phases at the interface in the cooling process (Ref 30). The microstructure of the TiB_2/Cu-0.5Cr (VAM) composite is shown in Fig. 1(g). The TiB_2 particles were dispersed uniformly. The raw Cr particles were dissolved into the copper matrix during vacuum arc smelting. During the vacuum arc melting process, the heat produced by the arc can melt the copper and ensured that the Cr particles were completely dissolved in the copper liquid. After the electrode melted, it was dropped into the water-cooled copper crystallizer and cooled rapidly to form a compact TiB_2/Cu-0.5Cr (VAM) composite without component segregation. The microstructure of the TiB_2/Cu-0.5Cr (VAM) composite aged at 475 °C for 4 h is shown in Fig. 3. Before and after vacuum arc melting, the TiB_2 particles maintained their original morphology without obvious agglomeration. It appears that TiB_2 particles were distributed uniformly, and the composite had no pores or other defects, as shown in Fig. 3.

TEM and a high-angle annular dark-field scanning TEM (HAADF-STEM) were used to study the interface and Cr precipitate distribution, as shown in Fig. 4. It can be seen in Fig. 4(a) that the interface between TiB_2 particles and the copper matrix was very clean, which indicates that interface bonding was good. Zou et al. (Ref 31) found that there was no obvious orientation relationship between copper and TiB_2 particles. The orderly distribution of twin boundaries is shown in Fig. 4(b). The twin boundaries acted as strong obstacles to the dislocation motion, leading to elevated strength (Ref 32).

The HAADF-STEM image, energy-dispersive x-ray (EDS) line scan and corresponding elemental mapping images of the composite are shown in Fig. 4(c) and (d). The EDS line scan in Fig. 4(d) shows that there was atomic interdiffusion between the copper matrix and TiB_2 particles. The line scan also confirmed that there was a well-bonded interface between the TiB_2 particles and the copper matrix. As seen in Fig. 4(g), the Cr particles were distributed uniformly in the copper matrix, and the particle size was less than 20 nm. The dislocations and subgrain boundaries were pinned by nano-Cr precipitates, which improved the strength and hardness of the composite.

3.3 Tensile Behavior of the TiB_2 Particle-Reinforced Cu/Cu-0.5Cr Composites

The engineering stress–strain curve of the TiB_2 particle-reinforced copper matrix composite measured at room temperature is shown in Fig. 5. The ultimate tensile strength (UTS), yield strength (YS) and elongation (EL) of the TiB_2 particle-reinforced copper matrix composite are listed in Table 1. Compared with TiB_2/Cu (PM) composites, the tensile strength of the TiB_2/Cu (VAM) composite increased by 8.8% to 246 Mpa; the elongation increased to 38.3%, and the plasticity of the composites increased greatly. The porosity significantly reduced the mechanical properties of the composites. However, compared with the powder metallurgy composite, the relative density of the composite prepared by vacuum arc melting

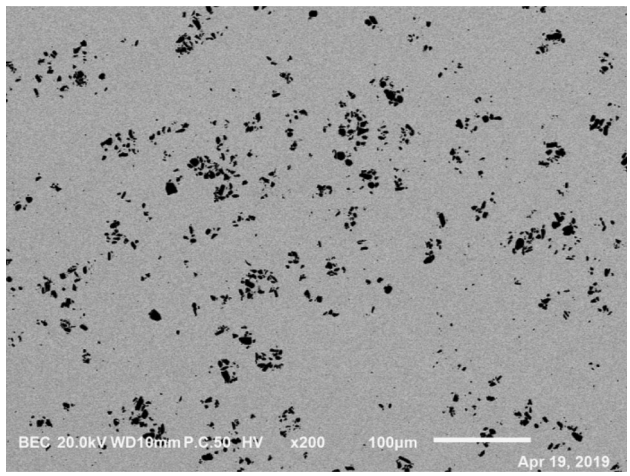

Fig. 3 Microstructures of TiB_2/Cu-0.5Cr (VAM) composite peak aging at 475 °C for 4 h

increased by 1.3 to 99.8%, as shown in Table 1. The vacuum arc melting technique can eliminate residual porosity in the sintering process and improve the interface bonding strength between TiB_2 particles and the copper matrix. Thus, VAM improved the strength and elongation of the composite.

The tensile strength of the TiB_2/Cu-0.5Cr (VAM) composite increased to 401 MPa, which was 63% higher than that of the TiB_2/Cu (VAM) composite, and the elongation decreased to 23.2%. Therefore, it was necessary to study the strengthening mechanism of the TiB_2/Cu-0.5Cr (VAM) composite. Compared with the TiB_2/Cu (VAM) composite, the increase in the composites strength was mainly due to the addition of Cr particles. In addition, a substantial number of dislocations did not bypass the TiB_2 particles by cutting or bowing-out mechanisms, while they accumulated at the interface of the TiB_2 particles, which increased the strength (Ref 33). The interaction between these dislocations and nano-Cr particles improved the composite strength. However, the TiB_2 particle diameter was more than 500 nm, and pinning dislocations were limited (Ref 21). Therefore, the TiB_2 particle contribution to strength was limited.

After aging of the composite, the Cr particles precipitated from the copper matrix, which effectively pinned the dislocations. The precipitation strengthening effect can be evaluated by Orowan strengthening (Ref 34, 35):

$$\Delta\sigma_{\text{Orowan}} = \frac{0.13 G_{\text{m}} b}{\lambda} \ln \frac{r}{b} \quad \text{(Eq 1)}$$

where G is the shear modulus (45.5 GPa), b is the Burgers vector (0.255 nm), r is the mean particle radius, and λ is the particle spacing (Ref 33). According to the parameters obtained

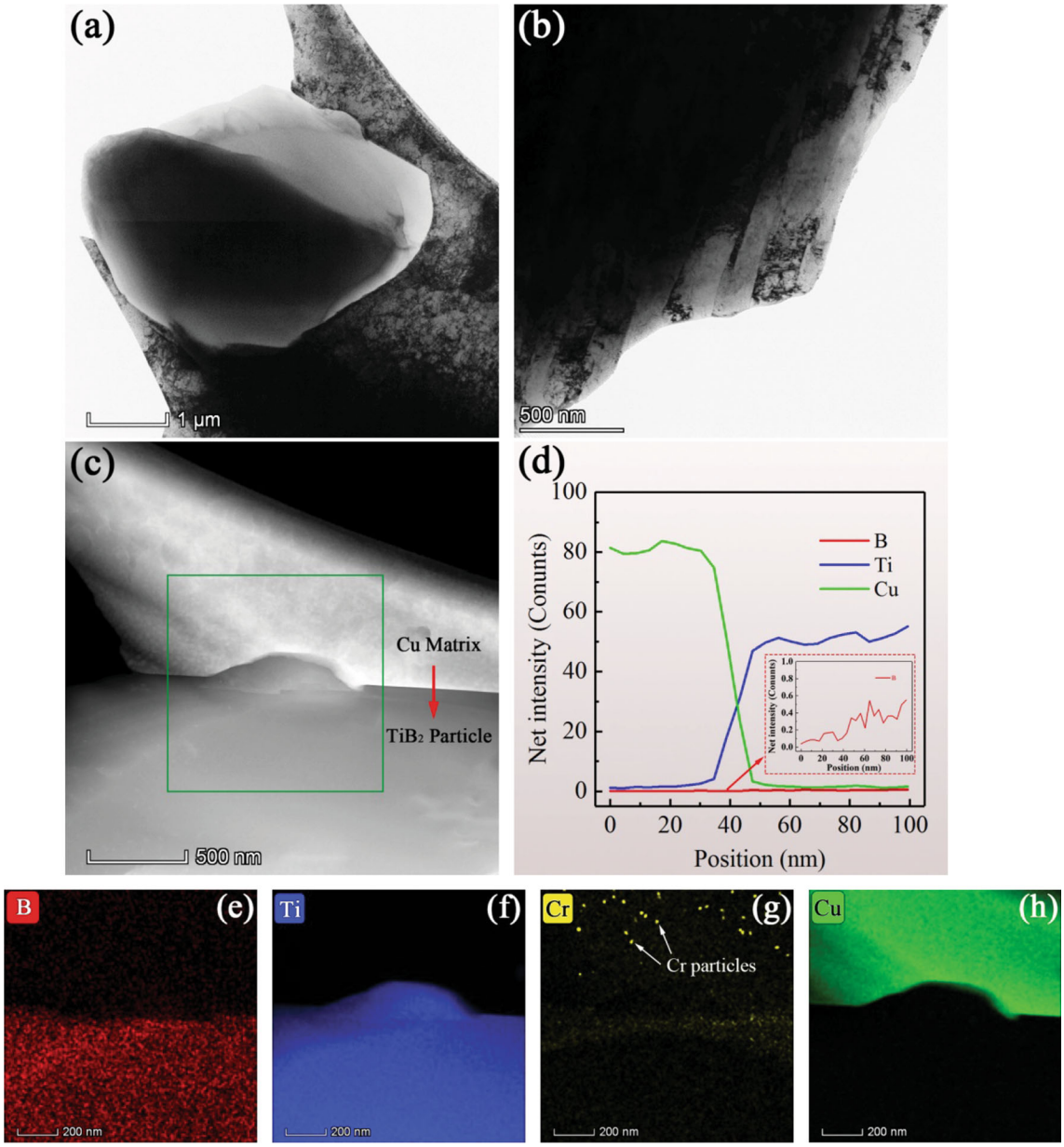

Fig. 4 TEM and HAADF-STEM images of TiB_2/Cu-0.5Cr (VAM) composite: (a) TiB_2 particle and copper matrix, (b) HRTEM image, (c) HAADF-STEM of TiB_2/Cu-0.5Cr (VAM) composite, (d) element line scans in the marked position in (c), and (e), (f), (g), (h) mapping scan (B, Ti, Cr, Cu) in the marked position in (c)

from the literature, the diameter of the Cr precipitates (approximately 20 nm) and the particle spacing (20-60 nm) are shown in Fig. 4(g). The results show that the Orowan strengthening contribution from the Cr particles was approximately 138.4 MPa. Therefore, Orowan strengthening is the main strengthening mechanism of the composites.

3.4 Failure Morphology and Mechanism of the Composites

The tensile sample for room temperature tests and for studying the fracture morphology of the TiB_2 particle-reinforced copper matrix composite is shown in Fig. 6. The macrofracture morphology of the tensile samples was a typical cup-cone fracture or necking fracture, both of which showed typical ductile fracture characteristics. As shown in Fig. 6(b), the TiB_2 particles were directly separated from the matrix during the tensile process due to the weak interface bonding of the composites prepared by powder metallurgy. TiB_2 particles were found at the bottom of the dimples, and small equiaxed dimples were densely distributed around them. The tensile macrofracture of the TiB_2/Cu (VAM) composite had an obvious necking phenomenon in Fig. 6(a), and TiB_2 particles were also distributed at the bottom of the dimples, as shown in Fig. 6(c). For the TiB_2/Cu (VAM) composite, the fracture dimples were large, and the tearing edge was rough, which allowed the composite to absorb additional energy during the tensile process and improve the strength and ductility of the material. In addition, the exposed TiB_2 particles were partially covered by copper, which indicates that the interface bonding was good. This finding also explains why the strength and elongation of the TiB_2/Cu (VAM) composite were better than those of the

TiB_2/Cu (PM) composite. Figure 6(d) shows the tensile fracture morphology of the TiB_2/Cu-0.5Cr (VAM) composite at peak aging. The fracture morphology mainly consisted of shear dimples, the tearing edge was smooth and the dimple size was reduced. The nano-Cr precipitates effectively impeded the dislocation movement, so the ultimate strength and yield strength at room temperature were improved. The plastic deformation ability of the composite decreased, which led to the resistance to internal necking and the formation of additional microscale holes, so the size of the dimples decreased.

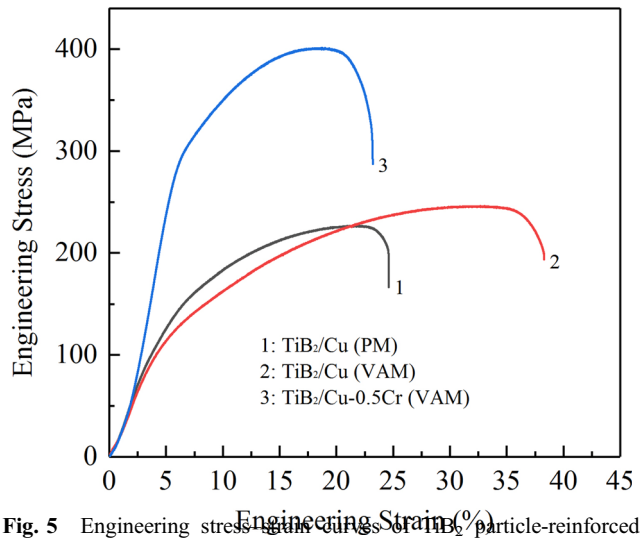

Fig. 5 Engineering stress–strain curves of TiB_2 particle-reinforced copper matrix composite

The tensile fracture failure mechanism of the TiB_2 particle-reinforced copper matrix composite is shown in Fig. 7. The black dot is a TiB_2 particle, and the arrow indicates the direction of the tensile load. During the tensile process, the deformation of the dispersed TiB_2 particles and copper matrix was uncoordinated, and the interfacial bonding was poor. Matrix–particle interface debonding led to the formation of microscale pores and an extension of the cracks. In addition, the cross section between adjacent microcavities decreased, and the stress increased, leading to dislocation movement toward the particles. When the accumulated elastic strain energy at the interface front was enough to overcome the interface binding force and form a new surface, a new microvoid was formed. The crack initiation and propagation of the composite started from the matrix–particle interface. Therefore, the interface bonding strength was the main factor affecting the mechanical properties of the copper matrix composite. It can be seen from the fracture morphology (Fig. 6) that the matrix–particle interface bonding strength of the composite prepared by vacuum arc melting was high, which can effectively prevent crack initiation and propagation. Furthermore, the dispersed nano-Cr precipitates blocked dislocations from moving to the matrix–particle interface during testing and reduced the elastic

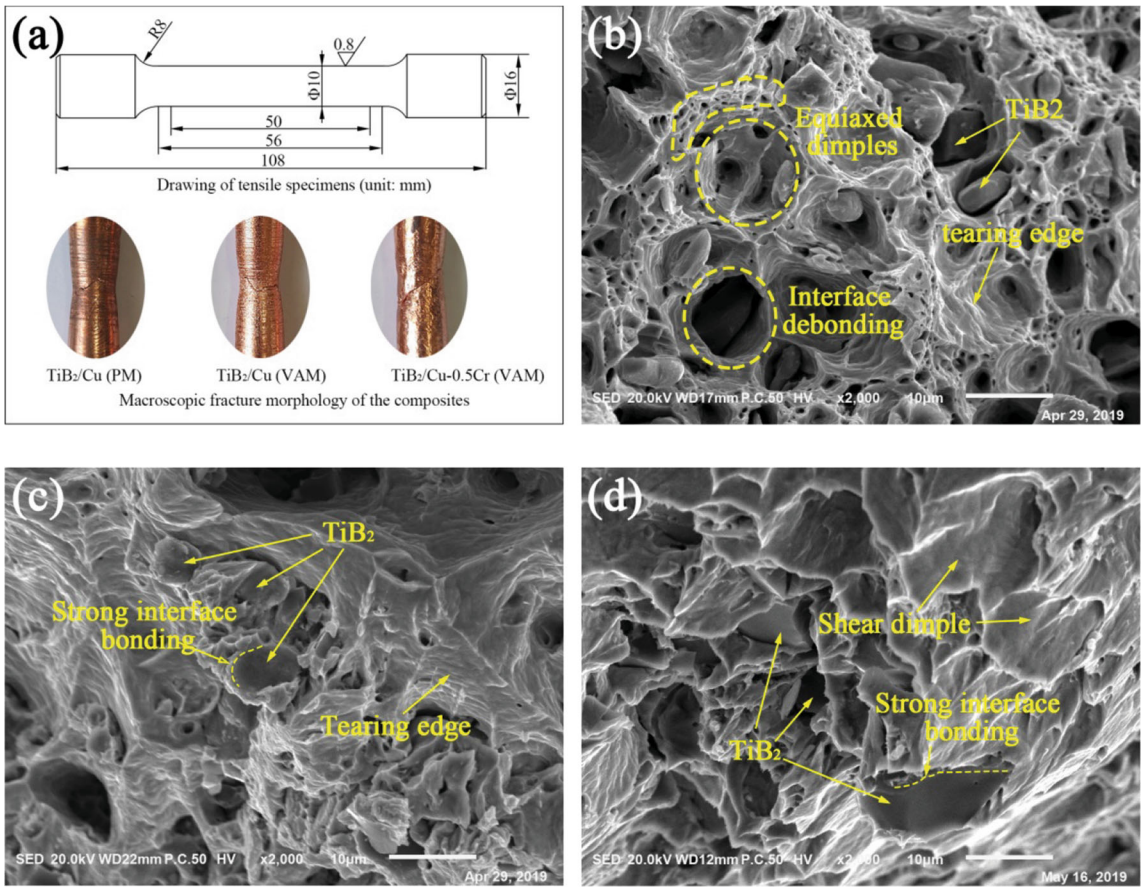

Fig. 6 SEM images of tensile fracture surfaces of composites (a) tensile sample and macroscopic fracture morphology, (b) TiB_2/Cu (PM) composite, (c) TiB_2/Cu (VAM) composite, (d) TiB_2/Cu-0.5Cr (VAM) composite

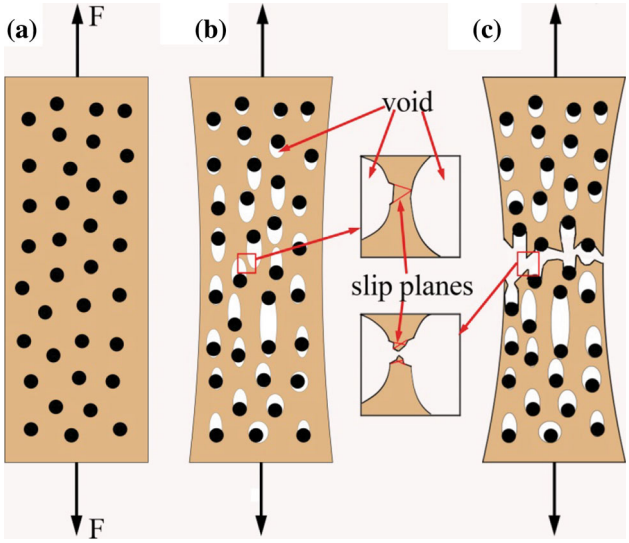

Fig. 7 Longitudinal tensile fracture model of TiB_2 particle-reinforced copper matrix composites

strain at the interface front. The dispersed nano-Cr precipitates also reduced the initiation and propagation of cracks and improved the strength.

4. Conclusion

In this study, the TiB_2 particle-reinforced Cu/Cu-0.5Cr composite was prepared by vacuum arc melting. The tensile strength of the TiB_2/Cu-0.5Cr (VAM) composite increased to 401 MPa, which was 63% higher than that of the TiB_2/Cu (VAM) composite, while the elongation and electrical conductivity decreased to 23.2 and 82.3% IACS, respectively. The strengthening mechanism of the TiB_2/Cu-0.5Cr (VAM) was via dislocation accumulation at the TiB_2 particles and Orowan strengthening of the Cr precipitates. The fracture mechanism of the composite was via matrix–particle interface debonding and nucleation, growth, agglomeration and fracture of cavities at the interface. The interface bonding strength was the main factor that impacted the mechanical properties of the composites.

Acknowledgments

This work was supported by the National Natural Science Foundation of China (Grant Nos. U1502274 and 51605146), Outstanding Talents Foundation of Henan Province (No. 182101510003), Key Projects of Henan Province (No. 20174GJPT1), China Postdoctoral Science Foundation (No. 2018M632769), and Henan Plan Project for College Youth Backbone Teacher (No. 2018GGJS045).

References

1. X.H. Guo, K.X. Song, S.H. Liang, Y. Zhou, and X. Wang, Relationship Between the MgO_p/Cu Interfacial Bonding State and the Arc Erosion Resistance of MgO/Cu Composites, *J. Mater. Res.*, 2017, **32**, p 3753–3760
2. Z.L. Zhao, Z. Xiao, Z. Li, W.T. Qiu, H.Y. Jiang, Q. Lei, Z.R. Liu, Y.B. Jiang, and S.J. Zhang, Microstructure and Properties of a Cu-Ni-Si-Co-Cr alloy with High Strength and High Conductivity, *Mater. Sci. Eng. A*, 2019, **759**, p 396–403
3. H.M. Mallikarjuna, C.S. Ramesh, P.G. Koppad, R. Keshavamurthy, and D. Sethuram, Nanoindentation and Wear Behaviour of Copper Based Hybrid Composites Reinforced with SiC and MWCNTs Synthesized by Spark Plasma Sintering, *Vacuum*, 2017, **145**, p 320–333
4. G.A. Bagheri, The Effect of Reinforcement Percentages on Properties of Copper Matrix Composites Reinforced with TiC Particles, *J. Alloys Compd.*, 2016, **676**, p 120–126
5. W. Zeng, J.W. Xie, D.S. Zhou, Z.Q. Fu, D.L. Zhang, and E.J. Lavernia, Bulk Cu-NbC Nanocomposites with High Strength and High Electrical Conductivity, *J. Alloys Compd.*, 2018, **745**, p 55–62
6. L. Lu, Y.F. Shen, X.H. Chen, L.H. Qian, and K. Lu, Ultrahigh Strength and High Electrical Conductivity in Copper, *Science*, 2004, **304**, p 422–426
7. K.M. Shu and G.C. Tu, The Microstructure and the Thermal Expansion Characteristics of Cu/SiC_p composites, *Mater. Sci. Eng. A*, 2003, **349**, p 236–247
8. X.H. Guo, K.X. Song, S.H. Liang, and C.H. Zheng, Thermal Expansion Behavior of MgO/Cu Composite with Lower MgO Volume Fraction, *Mater. Res. Bull.*, 2012, **47**, p 3211–3215
9. A. Fathy, Investigation on Microstructure and Properties of Cu-ZrO_2 Nanocomposites Synthesized by In Situ Processing, *Mater. Lett.*, 2018, **213**, p 95–99
10. A. Fathy, O. Elkady, and A. Abu-Oqail, Production and Properties of Cu-ZrO_2 Nanocomposites, *J. Compos. Mater.*, 2018, **52**, p 1519–1529
11. A. Fathy, O. Elkady, and A. Abu-Oqail, Microstructure, Mechanical and Wear Properties of Cu-ZrO_2 Nanocomposites, *Mater. Sci. Technol.*, 2017, **33**, p 2138–2146
12. S.H. Liang, W.Z. Li, Y.H. Jiang, F. Cao, G.Z. Dong, and P. Xiao, Microstructures and Properties of Hybrid Copper Matrix Composites Reinforced by TiB Whiskers and TiB_2 Particles, *J. Alloys Compd.*, 2019, **797**, p 589–594
13. J. Feng, S.H. Liang, K.X. Song, X.H. Guo, Y. Zhang, G.H. Li, and A.A. Volinsky, Effects of Particle Characteristic Parameters on the Electrical Conductivity of TiB_2/Cu Composites: A Modified Model for Predicting Their Electrical Conductivity, *J. Mater. Eng. Perform.*, 2019, **28**, p 4316–4323
14. A. Nagesha, P. Parameswaran, A. Biswas, R. Sandhya, A.K. Asraff, and M.D. Mathew, Microstructural Investigations into the Low Cycle Fatigue Deformation of a Cu-Cr-Zr-Ti Alloy, *Mater. Sci. Eng. A*, 2013, **582**, p 91–95
15. C.L. Zou, H.J. Kang, W. Wang, Z.N. Chen, R.G. Li, X.X. Gao, T.J. Li, and T.M. Wang, Effect of La Addition on the Particle Characteristics, Mechanical and Electrical Properties of In Situ Cu-TiB_2 Composites, *J. Alloys Compd.*, 2016, **687**, p 312–919
16. J.H. You, A. Brendel, S. Nawka, T. Schubert, and B. Kieback, Thermal and Mechanical Properties of Infiltrated W/CuCrZr Composite Materials for Functionally Graded Heat Sink Application, *J. Nucl. Mater.*, 2013, **438**, p 1–6
17. A. Bahador, J. Umeda, E. Hamzah, F. Yusof, X.C. Li, and K. Kondoh, Synergistic Strengthening Mechanisms of Copper Matrix Composites with TiO_2 Nanoparticles, *Mater. Sci. Eng. A*, 2020, **772**, p 138797
18. H. Li, S.R. Yu, W.X. Xie, X.X. Han, and X.H. Wang, A Study About the Influence of Single-Scale and Dual-Scale Structures on Surface Wettability, *Appl. Phys. A*, 2017, **123**, p 374–382
19. J. Rösler and M. Bäker, A Theoretical Concept for the Design of High-Temperature Materials by Dual-Scale Particle Strengthening, *Acta Mater.*, 2000, **48**, p 3553–3567
20. K.Q. Song, Z.C. Lu, M. Zhu, R.Z. Hu, and M.Q. Zeng, A Remarkable Enhancement of Mechanical and Wear Properties by Creating a Dual-Scale Structure in an Al-Sn-Si Alloy, *Surf. Coat. Technol.*, 2017, **325**, p 682–688
21. C.L. Zou, Z.N. Chen, E.Y. Guo, H.J. Kang, G.H. Fan, W. Wang, R.G. Li, S.R. Zhang, and T.M. Wang, A Nano-Micro Dual-Scale Particulate-Reinforced Copper Matrix Composite with High Strength, High Electrical Conductivity and Superior Wear Resistance, *RSC Adv.*, 2018, **8**, p 30777–30782
22. A.M. Sadoun, A. Fathy, A. Abu-Oqail, H.T. Elmetwaly, and A. Wagih, Structural, Mechanical and Tribological Properties of Cu-ZrO_2/GNPs Hybrid Nanocomposites, *Ceram. Int.*, 2020, **46**, p 7586–7594

23. H.E. Mir, A. Jardy, J.-P. Bellot, P. Chapelle, D. Lasalmonie, and J. Senevat, Thermal Behaviour of the Consumable Electrode in the Vacuum Arc Remelting Process, *J. Mater. Process. Technol.*, 2010, **210**, p 564–572
24. S.M.Y. Kaku, V. Raju, K. Bharath, R.F. Godec, and H.R. Tiyyagura, Evaluation of ZrB_2 Reinforced Al/Al Alloy Composite Produced by Powder Metallurgy-Vacuum Arc Melting Technique: A Unique Approach, *Vacuum*, 2018, **155**, p 539–545
25. X.H. Yang, J.T. Zou, P. Xiao, and X.H. Wang, Effects of Zr Addition on Properties and Vacuum Arc Characteristics of Cu-W Alloy, *Vacuum*, 2014, **106**, p 16–20
26. R. Müller, Arc-Melted Cu-Cr Alloys as Contact Materials for Vacuum Interrupters, *Siemens Forsch. Entw.*, 1988, **17**, p 105–111
27. P. Li, Ai, X., W.B. Wang, X.J. Wang, G. Li, Micro-Structure and Performance of Vacuum Consumable Arc Melting Copper Chromium Contact Material, in *Proc. 3rd Int. Conf. Electr. Power Equip.-Switching Technol. (ICEPE-ST)*, p 538–540
28. C.D. Xia, W. Zhang, Z.Y. Kang, Y.L. Yan, Y.F. Wu, R. Zhang, G.Y. Xu, and M.P. Wang, High Strength and High Electrical Conductivity Cu-Cr System Alloys Manufactured by Hot Rolling-Quenching Process and Thermomechanical Treatments, *Mater. Sci. Eng. A*, 2012, **538**, p 295–301
29. A. Meng, J.F. Nie, K. Wei, H.J. Kang, Z.J. Liu, and Y.H. Zhao, Optimization of Strength, Ductility and Electrical Conductivity of a Cu-Cr-Zr Alloy by Cold Rolling and Aging Treatment, *Vacuum*, 2019, **167**, p 329–335
30. T.M. Gong, P.P. Yao, X. Xiong, H. Zhou, Z.Y. Zhang, Y.L. Xiao, L. Zhao, and M.W. Deng, Microstructure and Tribological Behavior of Interfaces in Cu-SiO_2 and Cu-Cr Metal Matrix Composites, *J. Alloys Compd.*, 2019, **786**, p 975–985
31. C.L. Zou, Z.N. Chen, H.J. Kang, W. Wang, R.G. Li, T.J. Li, and T.M. Wang, Study of Enhanced dry Sliding Wear Behavior and Mechanical Properties of Cu-TiB_2 Composites Fabricated by In Situ Casting Process, *Wear*, 2017, **392-393**, p 118–125
32. X.H. Zhang, Y. Zhang, B.H. Tian, J.C. An, Z. Zhao, A.A. Volinsky, Y. Liu, and K.X. Song, Arc Erosion Behavior of the Al_2O_3-Cu/(W, Cr) Electrical Contacts, *Compos. B*, 2019, **160**, p 110–118
33. P.C. Zhang, J.C. Jie, Y. Gao, H. Li, Z.Q. Cao, T.M. Wang, and T.J. Li, Preparation and Properties of TiB_2 Particles Reinforced Cu-Cr Matrix Composite, *Mater. Sci. Eng. A*, 2015, **642**, p 398–405
34. M. Habibnejad-Korayem, R. Mahmudi, and W.J. Poole, Enhanced Properties of Mg-based Nano-Composites Reinforced with Al_2O_3 Nano-Particles, *Mater. Sci. Eng. A*, 2009, **519**, p 198–203
35. S.A. Sajjadi, H.R. Ezatpour, and M.T. Parizi, Comparison of Microstructure and Mechanical Properties of A356 Aluminum Alloy/Al_2O_3 Composites Fabricated by Stir and Compo-Casting Processes, *Mater. Des.*, 2012, **34**, p 106–111

Publisher's Note Springer Nature remains neutral with regard to jurisdictional claims in published maps and institutional affiliations.